



**HAL**  
open science

## Reducing plasma-material interactions in the DIII-D low-Z and high-Z divertors with impurity powders

Florian Effenberg, Bortolon A., Abe S., Maingi R., Nagy A., Parsons M.S., Abrams T., Bykov I., Sinclair G., Thomas D.M., et al.

► **To cite this version:**

Florian Effenberg, Bortolon A., Abe S., Maingi R., Nagy A., et al.. Reducing plasma-material interactions in the DIII-D low-Z and high-Z divertors with impurity powders. 29th IAEA Fusion Energy Conference (FEC 2023), International Atomic Energy Agency (IAEA), Oct 2023, London, United Kingdom. hal-04253635

**HAL Id: hal-04253635**

**<https://hal.science/hal-04253635>**

Submitted on 23 Oct 2023

**HAL** is a multi-disciplinary open access archive for the deposit and dissemination of scientific research documents, whether they are published or not. The documents may come from teaching and research institutions in France or abroad, or from public or private research centers.

L'archive ouverte pluridisciplinaire **HAL**, est destinée au dépôt et à la diffusion de documents scientifiques de niveau recherche, publiés ou non, émanant des établissements d'enseignement et de recherche français ou étrangers, des laboratoires publics ou privés.



Distributed under a Creative Commons Attribution 4.0 International License

## REDUCING PLASMA-MATERIAL INTERACTIONS IN THE DIII-D LOW-Z AND HIGH-Z DIVERTORS WITH IMPURITY POWDERS

F. EFFENBERG, A. BORTOLON, S. ABE, R. MAINGI, A. NAGY, M.S. PARSONS  
Princeton Plasma Physics Laboratory  
Princeton, NJ, United States of America  
Email: feffenbe@pppl.gov

T. ABRAMS, I. BYKOV, G. SINCLAIR, D.M. THOMAS, H.Q. WANG  
General Atomics  
San Diego, CA, United States of America

R. DING  
Chinese Academy of Sciences  
Hefei, Anhui, People's Republic of China

H. FRERICHS  
University of Wisconsin - Madison  
Madison, WI, United States of America

F.M. LAGGNER  
North Carolina State University  
Raleigh, NC, United States of America

J.D. LORE  
Oak Ridge National Laboratory  
Oak Ridge, TN, United States of America

A.G. MCLEAN, F. SCOTTI, D. TRUONG  
Lawrence Livermore National Laboratory,  
Livermore, CA, United States of America

S.H. MESSER, J.D. MATEJA, J. REN  
University of Tennessee,  
Knoxville, TN, United States of America

U. LOSADA  
Auburn University,  
Auburn, AL, United States of America

Z. POPOVIC  
Oak Ridge Associated Universities  
Oak Ridge, TN 37830, United States of America

### Abstract

In the DIII-D tokamak, boron (B) and boron nitride (BN) powder injections have demonstrated effectiveness in mitigating heat fluxes and suppressing tungsten erosion and divertor leakage in closed divertor configurations without compromising core plasma performance. Upon integrating the small-angle slot (SAS) divertor with a W-coated outer ring (SAS-VW), the dynamics of impurity interactions became evident, showcasing the capability of low-Z impurity injections to counteract high-Z erosion. 25-50 mg/s BN powder increased the divertor neutral pressure up to 10-fold and reduced the peak parallel heat flux from 30 to 3 MW/m<sup>2</sup> in the divertor. BN powders emerged as superior dissipators, especially in closed divertors, compared to pure B powder. An experiment with a collector probe provided evidence that tungsten leakage from the SAS-VW reduced by 50% when measured at the outer midplane during boron powder injections. Both increases in boron and reduction in W were measured in the far scrape-off layer, suggesting that real-time boronization with powders can even be successful in those remote areas. The assessment of boron powder injection is supported by computational simulations using EMC3-EIRENE and the dust-injection simulator (DIS), which suggest that B deposition area increases for larger particle sizes. The modeling reveals these distinct effects in the deposition in the closed divertor under the assumption that re-erosion and redeposition are neglected. These findings underscore the promise of powder injection for managing plasma-material interactions in future fusion reactors, with potential enhancements via multiple toroidal injection points.

## 1. INTRODUCTION

The evolution of fusion reactors, including the forthcoming ITER and the projected US fusion pilot plant, depends on the effective management of the plasma-material interface, i.e., reducing the intense heat fluxes, preventing impurity sputtering, and high wall recycling [1, 2].

Current plasma-facing component (PFC) materials are compromised when subjected to continuous heat fluxes above  $10 \text{ MW/m}^2$ , as anticipated for these next-step devices [1]. Solutions under investigation include power dissipation via isotropic low-Z impurity line emission to prevent high heat fluxes to the divertor targets. Commonly, these low-Z impurities are introduced in a gaseous state to amplify divertor radiation or encase the core plasma with a radiative shield. This method, termed impurity gas seeding, has undergone extensive evaluation in machines like the tokamaks TEXTOR, JET, Alcator C-Mod, ASDEX-Upgrade, EAST, the heliotron LHD, and the stellarator W7-X [3-10]. In this approach, a radiative shield, in combination with divertor dissipation, mitigates PFC damage, setting the stage for prolonged long-pulse operations. Ideally, this approach would limit power losses at the boundary and divertor plasma, thus maintaining high core plasma performance. Low-Z impurities are, therefore, most suitable as they reduce temperatures mostly in the divertor, subsequently reducing the high heat and particle fluxes to the target and promoting plasma detachment [11, 12]. ITER will not have intrinsic low-Z impurities that can function as radiators, as its divertor will be made of tungsten. Additionally, likely, the first wall will also be made of tungsten rather than beryllium. Consequently, injection of low-Z impurities will be necessary for energy dissipation.

Certain gases, such as nitrogen and neon, are effective for power dissipation. However, nitrogen presents complications in reactor contexts because of tritiated ammonia production, a potential contaminant for the uranium beds of the ITER tritium plant [13]. Consequently, impurity selection is contingent on radiation qualities and possible chemical limitations. Contemporary investigations suggest boron as a potential alternative for radiative dissipation [14]. Yet, the introduction of gaseous boron is challenging due to potential hazards associated with compounds like diborane.

A novel technique involves the injection of low-Z solid materials, such as powders or granules. Recent implementations have focused on wall conditioning, disruption mitigation, and edge localized mode (ELM) control using boron, boron nitride, and lithium powders [15-22]. This method of powder injection proves especially advantageous for conditioning during long-pulse operation, particularly when using superconductive coils, offering an alternative to conventional glow discharge boronization. Moreover, the utilization of low-Z material injections for re-establishing low-Z wall claddings is being considered for alternative material solutions in fusion pilot plants [23].

Progress in real-time wall conditioning (RTWC) techniques has been enhanced by the development of the impurity powder dropper (IPD), enabling the injection of various impurity powders into the SOL of fusion plasmas. The present investigation focuses on boron and boron nitride powder injection, emphasizing its importance in wall conditioning at DIII-D. The aim of this study is to develop an understanding of boron atom transport and deposition post-injection and the subsequent evaluation of their uniform spread on the main plasma-facing components. Such information is crucial when evaluating the suitability of this method for advanced devices like ITER or W7-X. Considering the localized origin of impurities, and the relevance of 3D fields in both tokamaks and stellarators, the employment of the 3D plasma-fluid and kinetic neutral transport code EMC3-EIRENE in conjunction with a dust transport model is essential. Recent 3D full-torus simulations have provided insights into the transport and direct deposition of a local boron source in the DIII-D tokamak [24]. Corresponding simulations at LHD have shown such investigations also employing a dust transport model [25].

In the following, new results with low-Z powder injection in the new DIII-D V-shaped tungsten-coated small-angle slot divertor (SAS-VW) will be presented alongside progress made on 3D full-torus simulations incorporating a dust transport model.

## 2. MITIGATION OF PLASMA-MATERIAL INTERACTIONS IN THE FIRST DIII-D SLOT DIVERTOR

The impurity powder dropper, positioned atop the DIII-D tokamak, has four reservoirs filled with different impurity powders and is capable of directly introducing these powders into the OSP region [26]. In these experiments, the boron stands out due to its relatively large particle size of  $150 \text{ }\mu\text{m}$ , impacting its ablation

process (as will be shown in the modeling section). With the current setup in place, there is a delay of approximately 850 ms between actuation and the impurity powder reaching and impacting the divertor plasma.

The experiments conducted on the DIII-D tokamak have recently focused on upper single null (USN) configurations. In the upper single null, under ELMy H-mode conditions, a toroidal field ( $B_t$ ) was employed in both standard and reversed directions. Accompanied by a plasma current ( $I_p$ ) of 1.0 MA, a  $B_t$  of 2 T, a neutral beam power ( $P_{NB}$ ) of 6 MW, a normalized beta ( $\beta_n$ ) of 2.0, and an ELM frequency ( $f_{ELM}$ ) of  $\sim 80$  Hz, electron density ( $n_e$ ) was varied between  $3.6$  to  $5.0 \times 10^{19} \text{ m}^{-3}$ . This led to a distinct magnetic equilibrium with the outer strike point (OSP) being positioned in the SAS divertor. Depending on the  $B_t$  direction, the ion grad-B drift could point away from or into the SAS divertor. A visual representation of this equilibrium, including the OSP location at the SAS target and the powder injection point, can be found in Figure 1, which also details the impurity powder dropper device and a typical spatial B IV (465.8 nm) emissivity profile from ablating boron powder obtained by video diagnostics.

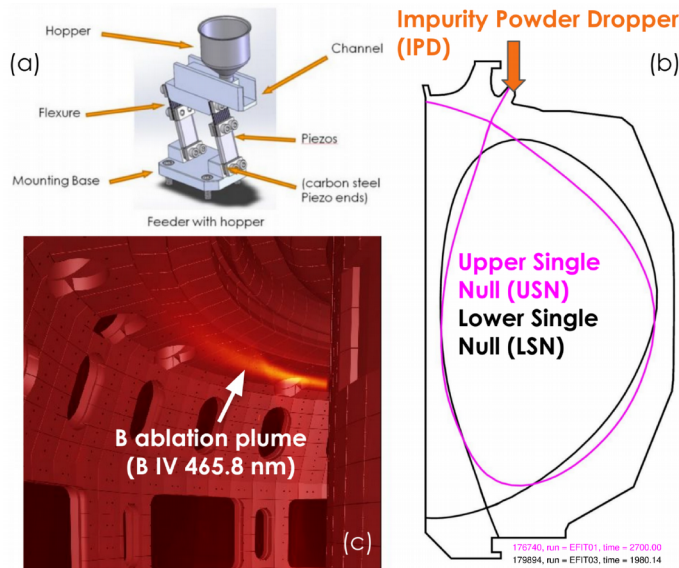


FIG. 1. (a) Impurity Powder Dropper (feeder) for powdered impurity material injection. (b) Magnetic configurations used for plasma-material interaction studies. The Upper Single Null (USN, magenta) configuration with the outer strike point located in the small-angle slot (SAS) divertor is used for divertor detachment studies. (c) shows material ablation for B powder injection with the periscope view.

Complementing this, the closed divertor geometry is beneficial as it inherently facilitates better dissipation of heat and particle fluxes due to enhanced neutral compression. The cooling behavior of various low-Z impurities in the dissipation experiments, such as lithium, boron, carbon, nitrogen, neon, and argon, is assessed through their radiative losses, incorporating factors like electron density, impurity density, and the power loss function.

The injection of boron, boron nitride, and lithium powders into the first graphite SAS divertor has been shown to substantially reduce heat fluxes and improve wall conditions [27]. Those experiments showed a substantial reduction in divertor heat flux ( $\sim 75\%$ ) and  $D_\alpha$  line emission ( $\sim 50\%$ ) during 3-35 mg/s Li, B, and BN powder injection without detrimental impact on core performance, demonstrating the core-edge compatibility of this technique.

Boron radiates at lower electron temperatures (1–10 eV) than lithium (10–100 eV). Boron nitride, combining boron and nitrogen properties, has been shown to most effectively dissipate divertor power in the first SAS divertor. These first experiments showed that compared to B powder, Li and BN powders generally performed better in enhancing the neutral compression and reducing the heat fluxes. However, very high BN rates had adverse effects, like decreased neutron rates. A cumulative deposition of 166 mg boron over four discharges improved wall pumping by more than an order of magnitude and reduced unwanted influxes of fuel and impurities from the walls and plasma-facing components. Those experiments showed very well the mitigation of plasma-material interactions of low-Z low recycling powders in the low-Z (graphite) closed SAS divertor.

After an upgrade and optimization of the SAS to a V-shaped geometry and tungsten-coated SAS-VW divertor [28, 29], the experiments have been repeated to study the effects of low-recycling powders on dissipation and high-Z divertor leakage. The IPD setup remains the same; however, plasma conditions and scenario have been slightly modified to let the OSP of the new divertor geometry and the inner ring of W-coated divertor tiles.

### 3. POWER DISSIPATION IN THE TUNGSTEN DIVERTOR WITH BORON AND BORON NITRIDE

After installing the SAS-VW divertor, which contains an outer ring of W-coated tiles, experiments were repeated with the outer strike point on the W surface. During this upgrade, the DIII-D carbon walls enabled

critical tests of impurity dynamics, such as preventing high-Z erosion by low-Z impurity injection. Boron (B) and boron nitride (BN) have been injected for divertor dissipation into the upper tungsten-coated small angle slot divertor in DIII-D during high confinement plasma operation. The H-mode plasma was operated with a plasma current of 1 MA and an on-axis toroidal field of 2 T, which was in the reversed  $B_t$  direction (ion  $B \times \nabla B$  directed into the divertor), favorable for H-Mode access. The plasma was heated through neutral beam injection at 7.4 MW and an on-axis electron-cyclotron resonance heating (ECRH) of 0.4 MW at a density of  $5\text{-}6 \times 10^{19} \text{ m}^{-3}$ . The ECRH was employed to prevent on-axis tungsten accumulation.

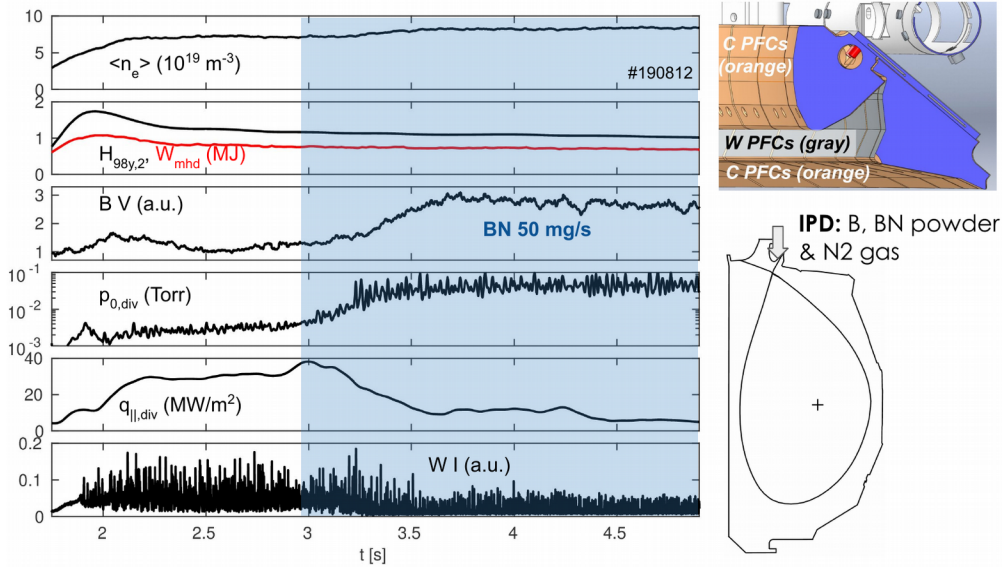


FIG. 2. (Left) Time traces for H-mode discharge with 50 mg/s boron nitride powder injection in SAS-VW divertor with outer strike point on the tungsten-coated tiles. Panels from top to bottom: line averaged electron density,  $H_{98y,2}$ , stored energy  $W_{mhd}$ , B V impurity line emission, divertor neutral pressure  $p_{0,div}$ , divertor heat flux  $q_{||,div}$ , and tungsten source emission W I. (Right, top) Sketch of the SAS-VW divertor target geometry [28]. (Right, bottom) The equilibrium separatrix and injection location for low-Z impurity powders with the impurity powder dropper (IPD).

Injection of boron powder at rates up to 25 mg/s into the SAS-VW divertor showed no substantial reduction in heat flux but an  $\sim 20\%$  decrease in neutron rates and stored magnetic energy. In the SAS-VW scenario, 25-50 mg/s BN powder increased the divertor neutral pressure up to 10-fold and reduced the peak parallel heat flux from 30 to 3 MW/m<sup>2</sup> measured near the IPD injection location with Langmuir probes, as shown in Fig. 2. A moderate fueling effect occurs while the confinement parameters are almost unaffected. The results also show that BN powder thus far serves as an effective dissipator in both the original SAS divertor with all-carbon walls and the high-Z SAS-VW divertor during USN H-mode scenarios. BN powder was also found to be a more effective dissipator than pure B powder in the closed divertor at comparable rates.

#### 4. REDUCING DIVERTOR TUNGSTEN LEAKAGE WITH REAL-TIME BORON INJECTION

The new SAS-VW divertor allowed the effect of real-time boron powder injection on tungsten divertor leakage to be studied. For this purpose, a graphite collector probe was inserted into the far-SOL through the midplane material evolution system (MiMES) to measure boron and tungsten deposition profiles during B powder injection. The probe has two flat sides, analyzed individually: one labeled "inner target facing" (ITF) and the other "outer target facing" (OTF), based on their magnetic connection to the inner and outer divertor targets [1]. Boron was injected at a rate of 3 mg/s in discharge #190790 from 2-5 seconds during the H-mode flat top phase.

Post-mortem analysis showed that B deposition was increased by over 100% during B injection, while W deposition was reduced by up to 50% on both ITF and OTF (Figure 2). The tungsten divertor leakage, the amount of tungsten measured on the probe divided by the spectroscopically measured erosion rate, was found to be reduced by a factor of 2 with boron injection. Those effects were measured in the distant scrape-off layer about 8 cm beyond the radial separatrix location. This remote SOL domain is also defined by in-vessel components acting as limiters and thus creating a complex 3D geometry of relatively short connection lengths.

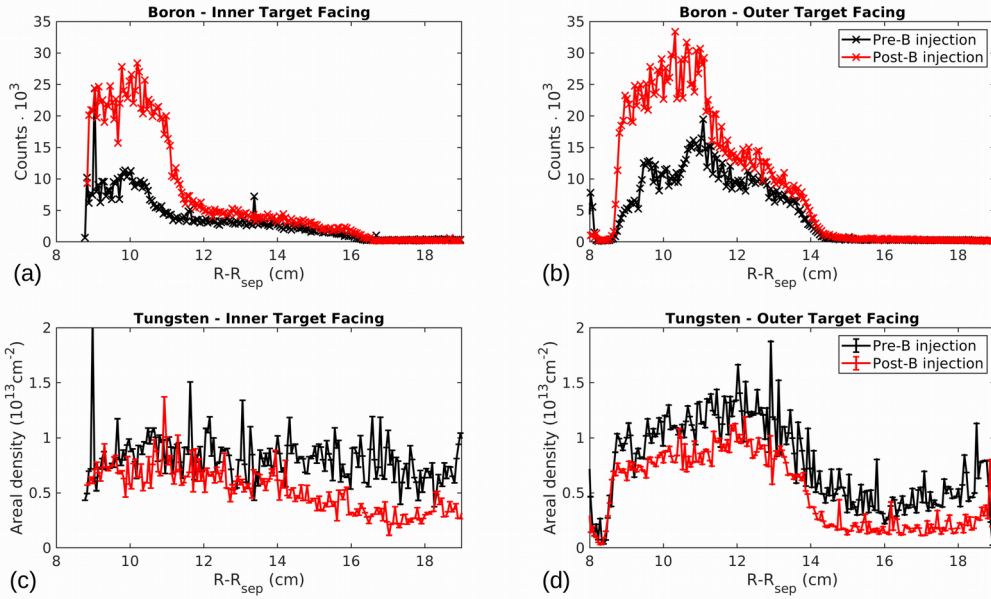


FIG. 3. Profiles obtained on collector probes during post-mortem analysis (a) boron on the inner target facing Midplane collector probe (MCP-ITF), (b) boron on the outer target facing Midplane collector probe (MCP-OTF), (c) tungsten (W) profile on the MCP-ITF, and (d) tungsten (W) profile on the MCP-OTF. The W originates from the tungsten-coated small-angle slot divertor (SAS-VW), while B has been injected with the impurity powder dropper (IPD).

The boron injection experiment followed a series of experiments with neon gas injections that considered the dependence of W divertor leakage on the poloidal impurity injection location [31]. The results presented in this study show not only that boron powder injected into the SAS-VW divertor reduces W divertor leakage but also that the boron deposition expands beyond the far divertor SOL into the remote limiter SOL. This suggests that powder injection may also be suitable for conditioning the main chamber walls. The W-coated tiles were removed after the campaign for surface analysis to study the deposition pattern and extent of boron transport from the injection location. Visible coatings on the W tiles were found during the tile inspection (Figure 4.). The surface layers were broader and denser, close to the impurity powder dropper (IPD) location, reduced in density, and spread further away in the toroidal direction.

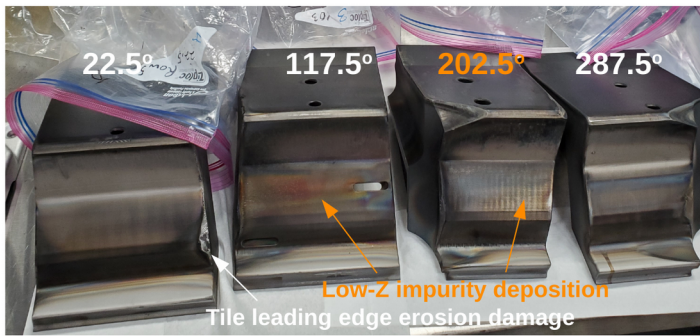


FIG. 4. Tungsten-coated tiles removed from the SAS-VW divertor from four toroidal locations: 22.5°, 117.5°, 202.5° and 287.5°. The IPD is located at 195°; i.e., the primary boron source is closest to the 202.5° tile. The tiles show leading edge erosion damage to the W-coatings due to misalignment. The brown and dark layers are low-Z impurity deposits likely from carbon and injected boron powder. The tiles will be further analyzed for boron migration and deposition studies.

## 5. PROGRESS ON INTEGRATED MODELLING OF IMPURITY POWDER INJECTION AND DIRECT DEPOSITION WITH EMC3-EIRENE AND THE DUST INJECTION SIMULATOR

A full-torus field-aligned computational grid was created based on a representative upper single null equilibrium to study the effects of local powder injection using the EMC3-EIRENE and the Dust Injection Simulator (DIS). EMC3-EIRENE is a fully 3D plasma-fluid and kinetic neutral edge transport code [32]. In the first step, clean deuterium plasma simulations have been carried out for a representative plasma scenario. The computational grid and main input parameters are shown in Figure 5 (a). The DIS code is used to model the ablation and transport of injected powder (or dust) particles [33]. Previous simulations have been used to model the effect of single B point sources as an EMC3-EIRENE standalone approach. In the present study, the complete dust

trajectories and powder ablation resulting from boron powder particles injected at a rate of 5 mg/s have been calculated. The heating source defined at the inner plasma boundary was set to 6 MW, and the separatrix density was set to  $1.5 \times 10^{19} \text{ m}^{-3}$ . The dust trajectories for two different powder particle sizes projected into the toroidal cross section at the injection location is shown in Figure 5 (b, c). The two examples show that smaller (lighter) dust particles ( $45 \mu\text{m}$ ) can be ejected outwards into the vacuum region as a result of the centrifugal force, while larger (heavier) particles ( $150 \mu\text{m}$ ) are penetrating deeper into the boundary plasma in the vertical direction due to the gravitational force [34].

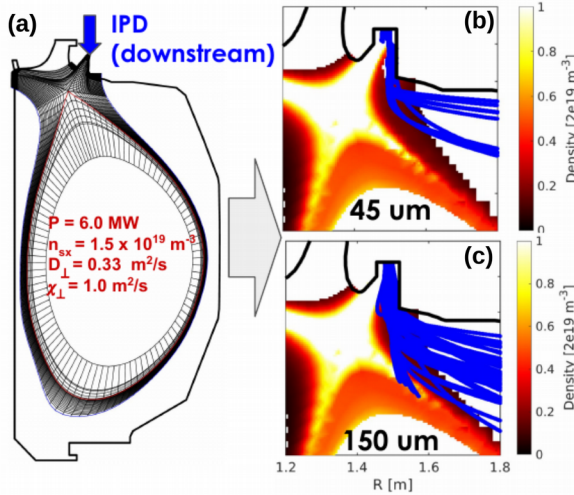


FIG. 5. Results from full-torus modeling with the 3D EMC3-EIRENE and DIS codes. (a) The computational grid and main input parameter used for boundary plasma transport simulations. Dust particles are introduced into the small-angle slot (SAS) divertor at the IPD location. (b) Background electron density distribution and dust trajectories (blue) for small ( $45 \mu\text{m}$ ) boron powder particles injected into the SAS. (c) Background electron density distribution and dust trajectories (blue) for larger ( $150 \mu\text{m}$ ) boron powder particles injected into the SAS. Note that the port gap included in the DIS divertor geometry at the IPD injection location results in a rectangular divertor shape that allows the powder particles to fall into the plasma without colliding with the outer edge of the SAS divertor.

Both  $45 \mu\text{m}$  and  $150 \mu\text{m}$  size B powders are usually used in experiments. In the simulations, the direct deposition of boron was calculated by mapping the boron fluxes onto the divertor targets. The simulation shows that the local injection of boron powder generally results in a toroidally localized deposition of B near the injection location under the simplifying assumption of no reerosion and redeposition. This simplifying assumption allows us to investigate the effect of the source location and the powder particle size on the ultimate deposition of low-recycling coatings. The distribution of boron impurities in the upper divertor region and the mapping of B fluxes onto the upper small-angle slot divertor plates are shown in Figure 6. The B impurity ion distributions and flux mappings show that smaller ( $45 \mu\text{m}$ ) particles are fully ablated and deposit in the vicinity of the injection location, while larger ( $250 \mu\text{m}$ ) particles can escape the SAS divertor before getting fully ablated and therefore show a larger toroidal spread in their deposition pattern.

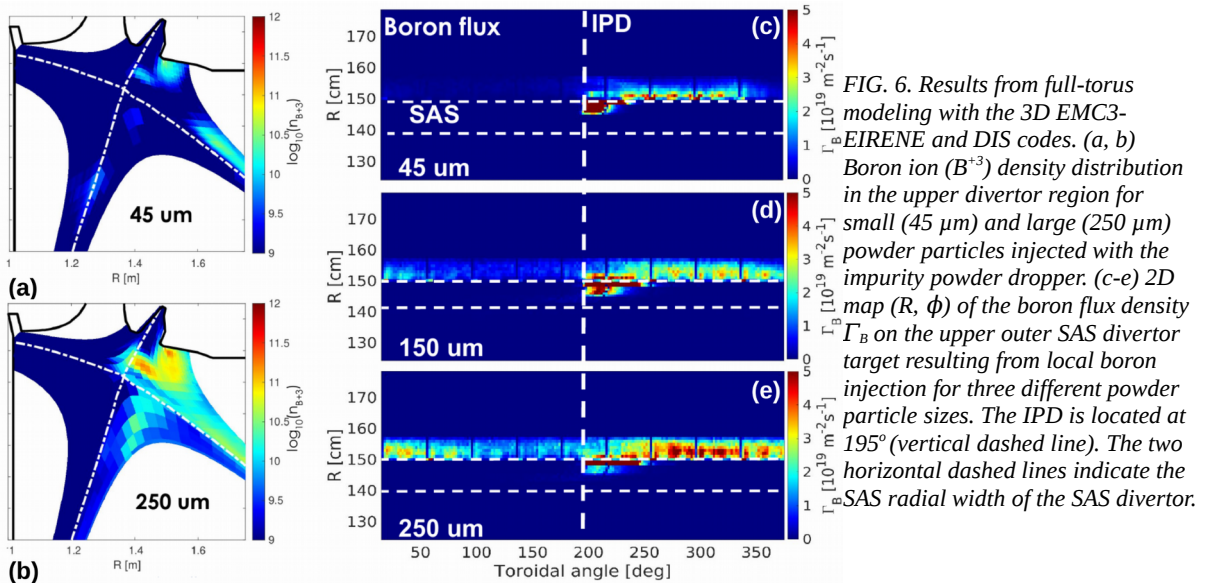


FIG. 6. Results from full-torus modeling with the 3D EMC3-EIRENE and DIS codes. (a, b) Boron ion ( $\text{B}^{3+}$ ) density distribution in the upper divertor region for small ( $45 \mu\text{m}$ ) and large ( $250 \mu\text{m}$ ) powder particles injected with the impurity powder dropper. (c-e) 2D map ( $R, \phi$ ) of the boron flux density  $\Gamma_B$  on the upper outer SAS divertor target resulting from local boron injection for three different powder particle sizes. The IPD is located at  $195^\circ$  (vertical dashed line). The two horizontal dashed lines indicate the SAS radial width of the SAS divertor.

The asymmetries in the boron flux deposition are due to the neglect of erosion and redeposition of B, which will require further development of integrated modeling using codes like WallDYN and ERO [35, 36].

These results suggest that the powder particle size ultimately matters for the ultimate B deposition in upper single null scenarios with the dust source in the divertor. Previous modeling studies for lower single null scenarios with boron injected into the crown (upstream) showed that the boron flux distribution is nearly unaffected by the particle size and penetration depth of boron [24].

## 6. SUMMARY AND CONCLUSIONS

This study presents findings based on the real-time injection of impurity powders into H-mode plasmas in the DIII-D tokamak, focusing on upper single null (USN) configurations. The introduction of boron, boron nitride, and lithium powders into the first graphite SAS divertor substantially reduced heat fluxes and improved wall conditions and served as a reference.

Subsequent upgrades to the SAS into a V-shaped geometry and a tungsten-coated SAS-VW divertor prompted repeat experiments to discern the effects of low-recycling powders on dissipation and tungsten divertor leakage. Post-upgrade, experiments on the SAS-VW divertor indicated that boron nitride (BN) served as an effective dissipator in both the original and the high-Z SAS divertors, with BN showing higher efficacy than pure boron.

Moreover, real-time boron injection on the new SAS-VW divertor showcased the ability to reduce tungsten leakage. Analyses revealed increased boron deposition and decreased tungsten deposition during boron injection, with effects prominent in the distant scrape-off layer. Boron deposition extended beyond the divertor into the remote limiter SOL.

Computational modeling efforts were made to study the effects of local powder injection using the EMC3-EIRENE and the Dust Injection Simulator (DIS) codes. These simulations aimed to understand the impact of boron powder particle size on its deposition pattern in the divertor. Results highlighted the significance of particle size in boron deposition, with smaller particles depositing closer to the injection location, while larger particles showed a more spread-out deposition pattern.

This study underscores the efficacy of low-Z low-recycling powders in managing tungsten divertor leakage and plasma-material interactions, with particle size critically influencing deposition patterns. The study demonstrates that powder injection is suitable for suppressing erosion and promoting detachment in carbon and tungsten environments in future fusion devices. Multiple injection points could balance PMI effects in larger devices. Moreover, the results show that the impact of real-time boron powder injection extends into the remote area at the outboard midplane where the tungsten deposition has been significantly suppressed, indicating its potential use as a conditioning technique in an ITER full-W wall environment.

## ACKNOWLEDGEMENTS

This material is based upon work supported by the U.S. Department of Energy, Office of Science, Office of Fusion Energy Sciences, using the DIII-D National Fusion Facility, a DOE Office of Science user facility, under Awards DE-AC02-09CH11466, DE-FC02-04ER54698, DE-SC0020357, DE-AC05-00OR22725, DE-AC52-07NA27344, DE-SC0019256, and DE-SC0020093. Work supported by the National Natural Science Foundation of China under Contract No. 12022511.

Disclaimer: This report was prepared as an account of work sponsored by an agency of the United States Government. Neither the United States Government nor any agency thereof, nor any of their employees, makes any warranty, express or implied, or assumes any legal liability or responsibility for the accuracy, completeness, or usefulness of any information, apparatus, product, or process disclosed, or represents that its use would not infringe privately owned rights. Reference herein to any specific commercial product, process, or service by trade name, trademark, manufacturer, or otherwise does not necessarily constitute or imply its endorsement, recommendation, or favoring by the United States Government or any agency thereof. The views and opinions of authors expressed herein do not necessarily state or reflect those of the United States Government or any agency thereof.

## REFERENCES

- [1] PITTS, R.A et al, A full tungsten divertor for ITER: physics issues and design status, *Nucl. Mater.* **438** (2013) S48–56
- [2] BUTTERY, R.J. et al, The advanced tokamak path to a compact net electric fusion pilot plant, *Nuclear Fusion* **61** (4) (2021) 046028
- [3] MADDISON, G.P. et al, Moderation of divertor heat loads by fuelling and impurity seeding in well-confined ELMy H-mode plasmas on JET *Nucl. Fusion* **51** (2011) 042001
- [4] SAMM, U. et al, Radiative edges under control by impurity fluxes, *Plasma Phys. Control. Fusion* **35** (1993) B167–75
- [5] REINKE, M.L. et al, Effect of N<sub>2</sub>, Ne and Ar seeding on Alcator C-Mod H-mode confinement, *J. Nucl. Mater.* **415** (2011) S340–4
- [6] KALLENBACH, A. et al, Impurity seeding for tokamak power exhaust: from present devices via ITER to DEMO *Plasma Phys. Control. Fusion* **55** (2013) 124041
- [7] CASALI, L. et al, Improved core-edge compatibility using impurity seeding in the small angle slot (SAS) divertor at DIII-D, *Phys. Plasmas* **27** (2020) 062506
- [8] CHEN, J. et al, Radiative divertor behavior and physics in Ar seeded plasma on EAST, *Chin. Phys. B* **26** 2017 095205
- [9] MORISAKI, T. et al, Radiated power distributions in impurity-seeded plasmas in LHD, *J. Nucl. Mater.* **463** (2015) 640–3
- [10] EFFENBERG F., et al, First demonstration of radiative power exhaust with impurity seeding in the island divertor at Wendelstein 7-X, *Nucl. Fusion* **59** (2019) 106020
- [11] MATTHEWS G.F., Plasma detachment from divertor targets and limiters, *J. Nucl. Mater.* **220–222** (1995) 104–16
- [12] KRASHENINNIKOV, S.I. et al, Divertor plasma detachment, *Phys. Plasmas* **23** (2016) 055602
- [13] NEUWIRTH D. et al, Formation of ammonia during nitrogen-seeded discharges at ASDEX Upgrade, *Plasma Phys. Control. Fusion* **54** (2012) 085008
- [14] PIGAROV A.Y., Radiative detached divertor with acceptable separatrix Zeff, *Phys. Plasmas* **24** (2017) 102521
- [15] SERGEEV V.Y. et al, Lithium technologies for edge plasma control, *Fusion Eng. Des.* **87** (2012) 1765–9
- [16] BORTOLON, A. et al, Real-time wall conditioning by controlled injection of boron and boron nitride powder in full tungsten wall ASDEX Upgrade, *Nucl. Mater. Energy* **19** (2019) 384–9
- [17] BORTOLON, A. et al, Observations of wall conditioning by means of boron powder injection in DIII-D H-mode plasmas, *Nucl. Fusion* **60** (2020) 126010
- [18] GILSON, E.P. et al, Wall conditioning and ELM mitigation with boron nitride powder injection in KSTAR, *Nucl. Mater. Energy* **28** (2021) 101043
- [19] SUN, Z. et al, Real time wall conditioning with lithium powder injection in long pulse H-mode plasmas in EAST with tungsten divertor, *Nucl. Mater. Energy* **19** (2019) 124–30
- [20] MAINGI, R. et al, ELM elimination with Li powder injection in EAST discharges using the tungsten upper divertor, *Nucl. Fusion* **58** (2018) 024003
- [21] NESPOLI, F. et al, First impurity powder injection experiments in LHD, *Nucl. Mater. Energy* **25** (2020) 100842
- [22] LUNSFORD R. et al, Characterization of injection and confinement improvement through impurity induced profile modifications on the Wendelstein 7-X stellarator, *Phys. Plasmas* **28** (2021) 082506
- [23] STANGEBY, P.C. et al, Developing solid-surface plasma facing components for pilot plants and reactors with replenishable wall claddings and continuous surface conditioning: A. Concepts and questions *Plasma, Phys. Control. Fusion* **64** (2022) 055018
- [24] EFFENBERG, F. et al, 3D modeling of boron transport in DIII-D L-mode wall conditioning experiments, *Nucl. Mater. Energy* **26** (2021) 100900
- [25] SHOJI, M. et al, Full-torus impurity transport simulation for optimizing plasma discharge operation using a multispecies impurity powder dropper in the large helical device, *Contributions to Plasma Physics* **60** (2020) 5–6
- [26] NAGY, A. et al, A multi-species powder dropper for magnetic fusion applications, *Rev. Sci. Instrum.* **89** (2018) 10K121
- [27] EFFENBERG, F. et al, Mitigation of plasma-wall interactions with low-Z powders in DIII-D high confinement plasmas, *Nucl. Fusion* **62** (2022) 106015
- [28] ABRAMS, T. et al, Design and physics basis for the upcoming DIII-D SAS-VW campaign to quantify tungsten leakage and transport in a new slot divertor geometry, *Phys. Scr.* **96** (2021) 124073
- [29] ABRAMS, T. et al., Unraveling the physics of tungsten sourcing and leakage from a slot divertor configuration on DIII-D, 29th IAEA Fusion Energy Conference (2023)
- [30] DONOVAN, D.C. et al, Utilization of outer-midplane collector probes with isotopically enriched tungsten tracer particles for impurity transport studies in the scrape-off layer of DIII-D, *Review of Scientific Instruments* **89** (2018) 10I115
- [31] PARSONS, M.S. et al 2023 NME, submitted
- [32] FENG, Y. et al, Recent Improvements in the EMC3-Eirene Code, *Contrib. Plasma Phys.*, **54** (2014) (4–6) 426–431
- [33] NESPOLI, F. et al, Hyperdiffusion of dust particles in a turbulent tokamak plasma, *Physics of Plasmas* **28** (2021) (7) 073704
- [34] EFFENBERG, F. et al. EMC3-EIRENE modeling of toroidally-localized material injections and its effect on plasma-material interactions, 19th International Conference on Plasma-Facing Materials and Components for Fusion Applications (2023)
- [35] SCHMID, K. et al. Integrated modelling: Coupling of surface evolution and plasma-impurity transport, *Nucl. Mater. Energy* **25** (2020) 100821
- [36] ROMAZANOV, J. et al. Validation of the ERO2.0 code using W7-X and JET experiments and predictions for ITER operation, 29th IAEA Fusion Energy Conference (2023)